Comparison of GPS, Seismological, and Geological Observations of Andean Mountain Building

Eryn R. Klosko[1], Seth Stein[1], David Hindle[2], Jonas Kley[3], Edmundo Norabuena[4], Timothy Dixon[4], and Mian Liu[5]

The growth of the Andes appears to occur primarily via a process by which approximately 10% of the net convergence between the oceanic Nazca and continental South American plates is taken up by permanent crustal shortening. At present, the shortening is concentrated in the SubAndean foreland fold and thrust belt (FTB) that forms the Andes' eastern limit. Here, we compare how the shortening is manifested in three different types of data for the Central Andes which give complementary insights. GPS data show the present shortening over a very short time interval (the past few years). Seismicity spans a somewhat longer interval (tens of years), but reflects only the portion of the deformation that gives rise to earthquakes. Geological data average shortening and deformation over millions of years. The three data types yield similar directions of shortening, generally closer to the normal to the mountain belt than the convergence direction. GPS and geological data averaged over the past 10 Ma yield similar rates of about 10 ± 5 mm/yr. However, the shortening rate inferred from earthquakes is an order of magnitude less, implying that most of the shortening occurs aseismically unless it is taken up by rare great earthquakes.

1. INTRODUCTION

"We may confidently come to the conclusion that the forces which slowly and by little starts uplift continents, and those which at successive periods pour forth volcanic matter are identical. I believe that the frequent quakings of the earth are caused by the rending of the strata, necessarily consequent on the tension of the land when upraised..."

Charles Darwin, The Voyage of the Beagle

Visiting the Andes in 1832, Darwin marveled at the 20,000 foot peaks, admired their volcanic features, noted the presence of marine deposits and dramatic erosion at high elevations, observed the effects of a great earthquake on the Chilean coast, and recognized that the mountains resulted from a combination of uplift, erosion, volcanism, and earthquakes. Following the formulation of plate tectonics in the 1960's, it was recognized that the Andes were the consequence of convergence between the subducting Nazca plate and the overriding South American plate (Figure 1) [*Dewey and Bird*, 1970]. Hence they are the present type example of major continental mountain building in response to subduction of an oceanic plate, in contrast to the Himalayas which reflect continental collision.

[1]Department of Geological Sciences, Northwestern University, Evanston, illinois
[2]Geoforschungszentrum, Potsdam, Germany.
[3]Geologisches Institut, Universitaet Karlsruhe, Karlsruhe, Germany.
[4]Rosenstiel School for Marine and Atmospheric Sciences, University of Miami, Miami, Florida.
[5]Department of Geological Sciences, University of Missouri, Columbia, Missouri.

Plate Boundary Zones
Geodynamics Series 30

10/1029/030GD07

However, the actual processes by which subduction of the oceanic plate causes uplift within the the continental plate are poorly understood and thus, are the subject of active investigation using various geological and geophysical techniques. It appears that the primary Andean mountain building process has been horizontal shortening [*Isacks*, 1988; *Dewey and Lamb*, 1992; *Allmendinger et al.*, 1997] which thickened the crust [*James*, 1971; *Zandt et al.*, 1996; *Yuan et al.*, 2000]. However, it appears that shortening alone may be insufficient [*Kley and Monaldi*, 1998], and that processes including magmatic addition [*Lamb and Hoke*, 1997; *James and Sacks*, 1999], lower crustal flow [*Kley and Monaldi*, 1998], and deep mantle flow [*Russo and Silver*, 1996] may also contribute. In this view, the high Altiplano plateau should be largely stable at present because shortening by thrust faulting and folding has migrated eastward to its present locus in the Eastern Cordillera and SubAndean foreland fold and thrust belt [*Sheffels*, 1990; *Sempere et al.*, 1990; *Gubbels et al.*, 1993; *Schmitz*, 1994; *Horton*, 1999; *Gregory-Wodzicki*, 2000; *Hindle et al.*, 2002]. These data are in general accord with the idea that crustal shortening uplifts a plateau to an equilibrium height, after which the plateau grows outward [*Molnar and Lyon-Caen*, 1988], although in detail it appears that the SubAndean deformation began before the plateau reached its full height [*Gubbels et al.*, 1993].

Our goal here is to compare the view of the shortening in the Central Andes given by three different data types: site velocities derived using the Global Positioning System (GPS), earthquake focal mechanisms, and geological reconstructions. The first two provide a present "snapshot" of the shortening, whereas the third gives the shortening over longer periods of time. Although the measurements are physically very different, they can be compared by deriving strain rate fields for each. As we will see, the different data types give complementary insights.

2. GPS OBSERVATIONS

We first consider the horizontal velocity field derived from measurements using GPS. Figure 1 shows the distribution of motion across part of the plate boundary zone extending from the stable interior of the oceanic Nazca plate, across the Peru-Chile trench to the coastal forearc, across the high Altiplano plateau and SubAndean foreland thrust belt, and into the stable interior of the South American continent [*Norabuena et al.*, 1998]. This area spans the major oroclinal bend near 18°, where the Andes change width and orientation.

The site velocities (Figure 1) are relative to stable South America, and so would be zero if the South American plate were rigid and all motion occurred at the trench plate boundary. Their directions of motion are similar to the overall plate convergence direction inferred from either global plate motion model NUVEL-1A [*DeMets et al.*, 1994], which averages over the past 3 Ma, or GPS data [*Norabuena et al.*, 1998; 1999; *Angermann et al.*, 1999; *Sella et al.*, 2002], which yield a similar direction but slower convergence. However, the site velocities are highest near the coast and decrease relatively smoothly from the interior of the Nazca plate to the interior of South America. Although the precise GPS site velocities depend on the time span of data used (we are refining this velocity field using recently acquired data and *Bevis et al.* [2001] derive somewhat different values using these data along with a longer span of other data), the overall velocity field is robust.

The velocity field reflects a variety of different processes, each of which take up part of the net plate motion, as shown schematically in Figure 2. Much of the convergence is locked at the subduction interface, causing elastic strain of the overriding plate that will be released in large interplate thrust earthquakes like the 2001 M_w 8.4 trench earthquake which caused about 80 deaths and widespread damage in coastal Peru. Some of the locked strain may also be released in aseismic slip after such earthquakes. Another portion of the plate motion appears to occur by stable interseismic sliding at the trench, which does not deform the overriding plate. Some of the motion may be taken up in the Altiplano. The remainder, which we focus on here, occurs across the SubAndean fold-and-thrust belt (FTB), causing permanent shortening and mountain building. Some of this shortening occurs in earthquakes, and some may occur aseismically.

Starting with a velocity field, various approaches can be taken to estimate how the motion is partitioned. Hence our estimate of the shortening rate, the parameter of greatest interest here, depends on both the velocity field and the analysis approach. Figure 1 shows an interpretation of these data derived by inverting the velocities in the convergence direction assuming that they reflect locked slip at the trench and permanent deformation in the FTB [*Norabuena et al.*, 1998]. In this kinematic model, about half of the plate convergence (30-40 mm/yr) is locked at the trench, and about another 18-33 mm/yr occurs by stable interseismic sliding. The rest, about 14 ± 7 mm/yr, occurs across the FTB, causing permanent shortening and mountain building.

A second approach uses a dynamic model of the velocity field across the Andes expected from plate driving forces and topography [*Liu et al.*, 2000 and this volume]. This model predicts that the short-term velocity field closely resembles the GPS velocity profile across the Andes, because the model includes both permanent deformation and elastic deformation that will be recovered during future earthquakes. In contrast, the long-term velocity field, which

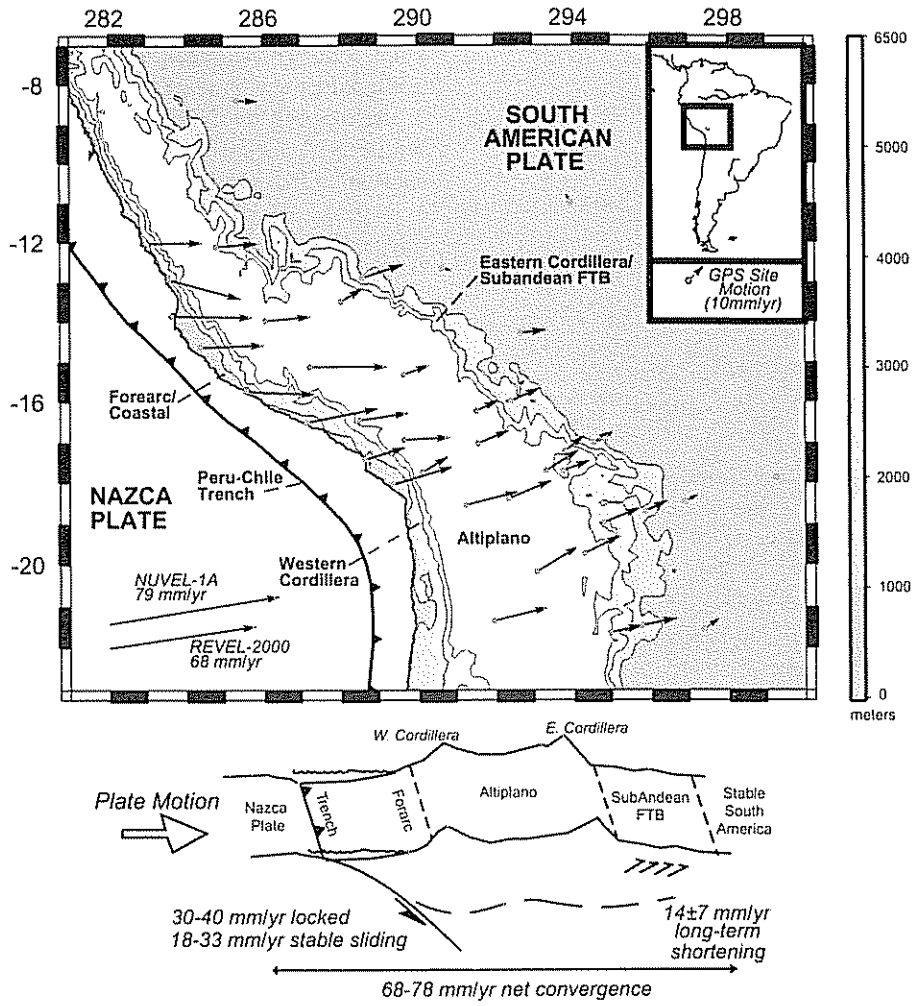

Figure 1. *Top* Major tectonic provinces of the Central Andes: the forearc/coastal region (from the Peru-Chile Trench to the Western Cordillera), the Western Cordillera, Altiplano (generally within the 3000 m contour elevation, below 10° S), and the Eastern Cordillera/SubAndean fold and thrust belt, FTB (generally from 1000-3000 m contour elevation, east of the Altiplano). GPS site velocities with respect to stable South America indicated by arrows [*Norabuena et al.* 1998], Nazca-South America relative convergence vectors are shown for NUVEL-1A [*DeMets et al.*, 1994] and the GPS-based model, REVEL-2000 [*Sella et al.*, 2002]. *Bottom* Cartoon showing the partitioning of the convergence between Nazca and South America plates as modeled with GPS data [*Norabuena et al.*, 1998], where part of total motion accumulates on locked portions of the plate interface at the trench, and is released when the interface ruptures in large thrust earthquakes, some occurs as stable (aseismic) sliding at the interface, and some causes permanent deformation via crustal shortening and mountain building.

reflects only the permanent deformation, predicts little long-term motion across the Andes but 10-15 mm/yr of concentrated long-term crustal shortening in the SubAndean fold-and-thrust zone.

Although it is convenient to give specific values for the convergence, locking, and shortening rates it is worth noting that these vary along strike, and that estimates of these parameters have significant uncertainties. From north (12°S) to south (23°S) of the study area, the predicted convergence rates vary from 75 to 80 mm/yr for NUVEL-1A and 64 to 69 mm/yr for REVEL-2000 [*Sella et al.*, 2002]. Uncertainties in the geodetic estimates of rates can come from at least three sources, all of which are difficult to assess. Those associated with the velocity field itself depend on assumptions about random and systematic errors in the GPS analysis [*Mao et al.*, 1999]. In general, these should be reduced by longer measurement intervals. Uncertainties due to the choice of model parameterizations are

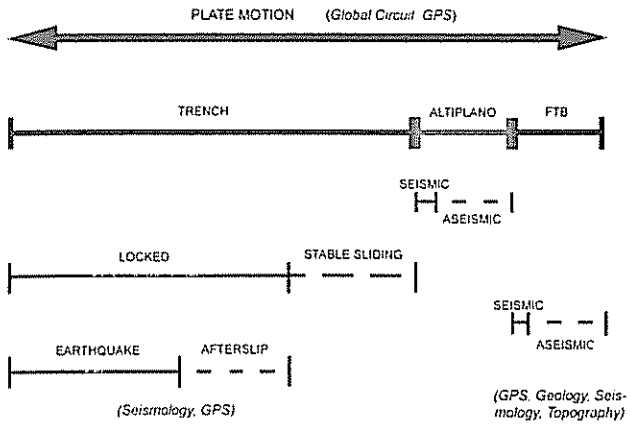

Figure 2. Schematic showing possible partitioning of plate motion within the boundary zone between the South America and Nazca plates and how the motions can be observed.

probably best assessed by comparing different parameterizations. Uncertainties in the fitting process, for an assumed velocity field and model parameterization, can be estimated from the fits to the data. However, these uncertainties do not include the effects of alternative velocity fields and model parameterizations, which can equally model the data. For example, *Bevis et al* [2001] find somewhat slower shortening using both a different velocity field and model parameterization. Hence, for our purposes here, we regard the GPS-derived shortening rate as about 10 ± 5 mm/yr, or about 5-15% of the net convergence.

In order to compare the geodetic data with the geological and earthquake data, we divide each into those for the Eastern Cordillera and FTB, and of the Altiplano, Western Cordillera, and coastal regions. We then divide these into groups depending on the available data. We anticipate deformation within these groups is essentially homogeneous [*Jackson and McKenzie,* 1988]. We derive a geodetic strain field for different portions of the study area. In each, we use the horizontal velocity components at different sites weighted by their uncertainty to estimate a common velocity gradient tensor whose symmetric part is the horizontal strain rate tensor [*Means,* 1990; *Feigl et al*, 1990]. Diagonalizing this tensor yields principal contraction ($\dot{\varepsilon}_2$) and extension ($\dot{\varepsilon}_1$) rates and azimuths for each group (Figure 3a, Table 1).

We expect the principal axes to reflect either the convergence direction itself or the resulting topography. To explore this issue, we use the direction from NUVEL-1A because this is independent of the GPS data (although, REVEL-2000 and NUVEL-1A agree in azimuth within 1°). As shown, the strain field within the FTB (groups 2-4) is dominated by shortening, with principal contraction axes closer to the perpendicular to the strike of the mountain belt than to the convergence direction (Figure 4). The smaller principal extension axes are oriented approximately parallel to the trend of the FTB. These observations are consistent with the idea that the velocity field largely represents the shortening that is building the mountains. In this case, stress axes in the FTB would be expected to reflect the topography, as shown in Figure 10 of *Liu et al* [this volume]. However, the principal contraction axis of group 1 is more similar to the convergence direction (Figure 4).

In contrast, sites within the Altiplano and coastal regions (groups 6 and 8) have maximum contraction axes more nearly parallel to the convergence direction than the to the normal of the mountain belt trend (Figure 4), although the FTB trend normal and convergence direction are similar in azimuth. This observation is consistent with the idea that the velocity field largely reflects elastic deformation due to the seismic cycle at the trench. The relation between the different directions for groups 5 and 7 is unclear. The extensional strain rate is an order of magnitude lower than the contractional, except in group 5.

3. GEOLOGIC OBSERVATIONS

The geodetic shortening rates of about 10 ± 5 mm/yr are comparable to those inferred geologically [*Norabuena et al*, 1998; *Lamb,* 2000]. For detailed comparison, we use a geologic velocity field synthesized from shortening observations for the past 25 Ma [*Hindle et al*, 2002; *Hindle and Kley,* this volume]. They find rates and directions of shortening for the past 10 Ma quite similar to the GPS data, which is gratifying given the independence of the techniques and the large difference in time scales.

Figure 3b and Table 1 show geologic strain rates inferred from the 0-10 Ma velocity field, which represents the time during which shortening migrated eastward to the FTB [*Isacks,* 1988; *Gubbels et al*, 1993]. The maximum contraction direction is perpendicular to the mountain belt, and so rotates clockwise south of the 18° bend (Figure 4). These directions and rates are similar to those shown by the geodetic data [*Hindle et al*, 2002].

4. EARTHQUAKE OBSERVATIONS

Deformation of the South American plate (or more strictly the continental portion of the plate boundary zone) is shown by shallow (≤ 60 km depth) seismicity landward of the trench. Figure 5 shows focal mechanisms for 53 earthquakes since 1968 from *Stauder* [1975], *Suarez et al* [1983], and Harvard CMT solutions. These were separated into those within the coast and Western Cordillera/Altiplano, and within the Eastern Cordillera/SubAndean FTB.

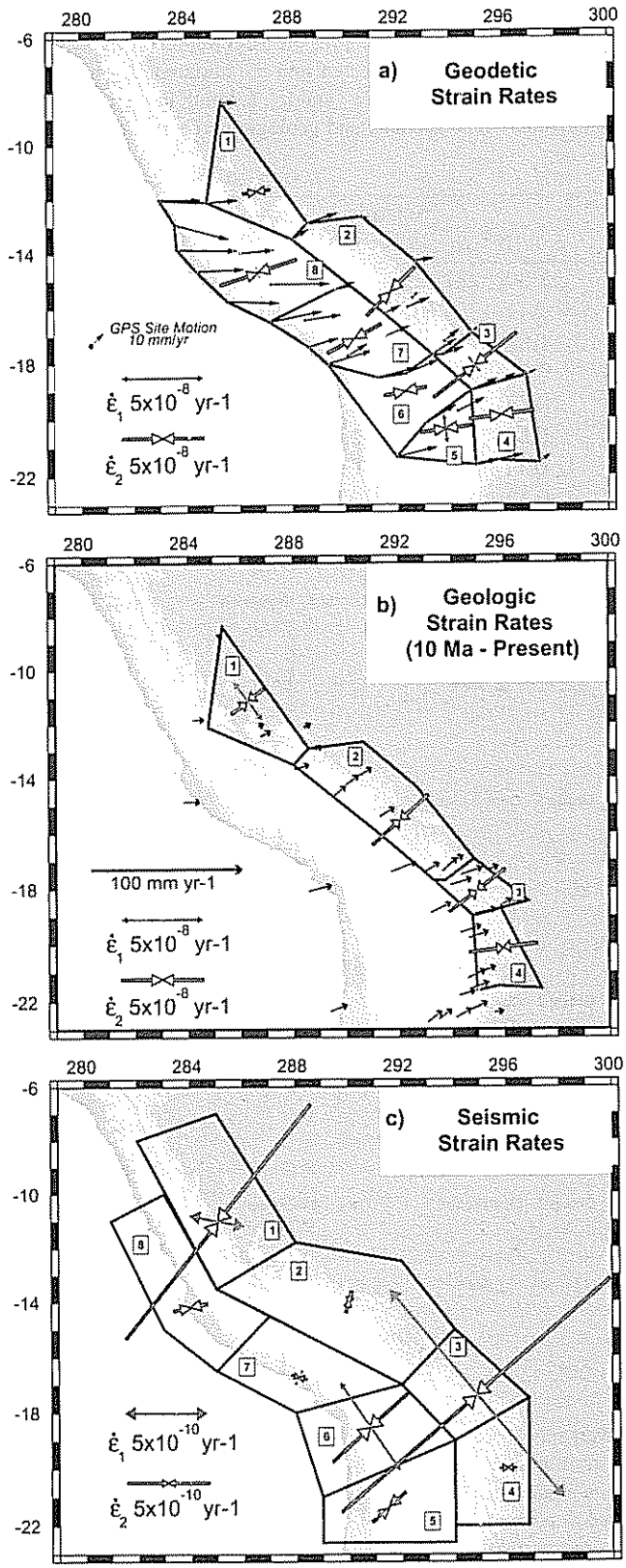

We then divided data from each region into groups. The number of earthquakes varies significantly between the groups, presumably because of the short sampling interval.

Following *Suarez et al* [1983] we use *Kostrov's* [1974] relation between the average strain rate, $\dot{\varepsilon}_{ij}$, and the moment tensors of the earthquakes, M_{ij}

$$\dot{\varepsilon}_{ij} = \frac{1}{2\,\mu\,V\,T_{obs}} \sum M_{ij}$$

where V is the assumed volume in which earthquakes occur, T_{obs} is the time interval (1968 - 2001), and μ is the rigidity (3.3×10^{11} dyne/cm^2). We assume that each group has a maximum faulting depth of 40 km. Although locally some events occur deeper, we use this estimate to represent an average depth of faulting for the entire region. As shown, the strain rate estimates are inversely proportional to the assumed average depth. Diagonalizing the strain rate tensor yields the eigenvalues associated with the principal contraction ($\dot{\varepsilon}_2$) and extension ($\dot{\varepsilon}_1$) axes (Figure 3c and Table 1). Because the seismic strain rate principal axes are three-dimensional, for comparison with the GPS and geologic results, they are shown in horizontal projection. Hence $\dot{\varepsilon}_2$ and $\dot{\varepsilon}_1$ can appear to be neither equal in magnitude nor orthogonal in direction.

Within the FTB (groups 1-4) from north to south (Figure 3c), the earthquakes show primarily thrust faulting, as expected. To the north and south of the 18°S bend thrust faulting mechanisms directly reflect the shortening. In the center strike-slip mechanisms, like that of the 1998 M_s 6.7 earthquake (17.60 S, 65.20 W) that caused approximately 100 deaths and damaged about 75% of the buildings in Aiquile, Bolivia, reflect block motions that accommodate shortening in the bend region [*Dewey and Lamb*, 1992]. The principal contraction axes in groups 3 and 4 are essentially perpendicular to the strike of the mountain belt, where as those in groups 1 and 2 are more oblique to both the FTB normal and the convergence direction. The large extensional axis nearly parallel to the mountain belt in group 3 results from the strike-slip mechanisms whose P-axes are

Figure 3*a*. Geodetic strain rate principal extension, $\dot{\varepsilon}_1$ and compression, $\dot{\varepsilon}_2$ axes for eight groups within the plate boundary zone GPS site velocities used to derive strain vectors for each group are shown. **3*b*:** Geologic strain rate results, in the same convention as above, for four groups of the FTB using data averaged over past 10 Ma [*Hindle et al*, 2002]. Geologic motions are shown by arrows. **3*c*:** Horizontal projection of seismic strain rate axes for eight groups within the plate boundary zone, plotted at a scale larger than for GPS and geologic results. These strain rate estimates are listed in Table 1. Topography scale is same as Figure 1.

Table 1. Horizontal geodetic, geologic (10 Ma - present) and seismic strain rate estimates. Geodetic results for South America GPS site velocities, weighted by each station velocity variance. Geologic results for the 10-0 Ma reconstruction from *Hindle et al.* [2002]. Seismic results for South American earthquakes, projected into the horizontal plane (according to plunge of strain axes). $\dot{\varepsilon}_1$ and $\dot{\varepsilon}_2$: strain rate magnitude in units of (1/yr). α_1 and α_2: azimuth in degrees east of north. Pl_1 and Pl_2: plunge in degrees with respect to horizontal. For geodetic and geologic horizontal strain rate, α_1 values are 90° from the listed α_2 values.

	Geodetic			Geologic			Seismic					
Group	$\dot{\varepsilon}_1 \times 10^{-8}$	$\dot{\varepsilon}_2 \times 10^{-8}$	α_2	$\dot{\varepsilon}_1 \times 10^{-8}$	$\dot{\varepsilon}_2 \times 10^{-8}$	α_2	$\dot{\varepsilon}_1 \times 10^{-9}$	α_1	Pl_1	$\dot{\varepsilon}_2 \times 10^{-9}$	α_2	Pl_2
1	-0.56	-1.66	82	2.9	-2.3	53	1.80	281	79	-1.78	39	5
2	-0.18	-3.98	45	-0.12	-4.4	48	0.17	7	71	-0.16	16	19
3	1.27	-6.24	53	-0.57	-4.1	53	1.62	320	3	-2.15	50	10
4	0.27	-3.90	83	-0.23	-4.1	83	0.10	326	81	-0.10	89	5
5	1.77	-3.07	83				0.37	49	47	-0.36	50	43
6	0.30	-2.56	80				0.67	326	12	-0.71	48	32
7	-0.33	-3.61	62				0.11	28	10	-0.16	103	55
8	0.77	-4.85	73				0.13	354	85	-0.21	78	1

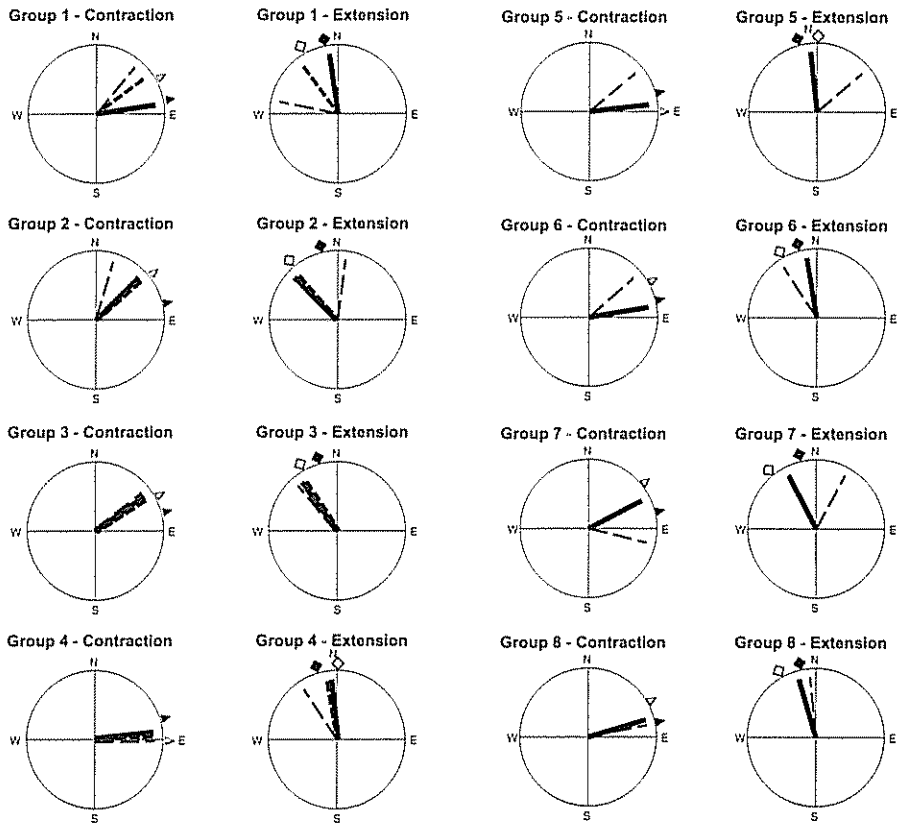

Figure 4. Azimuthal comparison of strain rate results with convergence direction (NUVEL-1A [*DeMets et al.*, 1994]) and trend of topography. Azimuths of the principal horizontal strain rates are indicated by lines *(geodetic, solid, geologic, short-thick dash; and seismic, long-thin dash)*. Contraction strain rate directions in each group are compared to the convergence direction *(solid triangle)* and the average normal direction to the trend of the topography *(open triangle)*. Extensional strain rate directions in each group are compared to the direction perpendicular to the convergence direction *(solid diamond)* and the average trend of the topography *(open diamond)*.

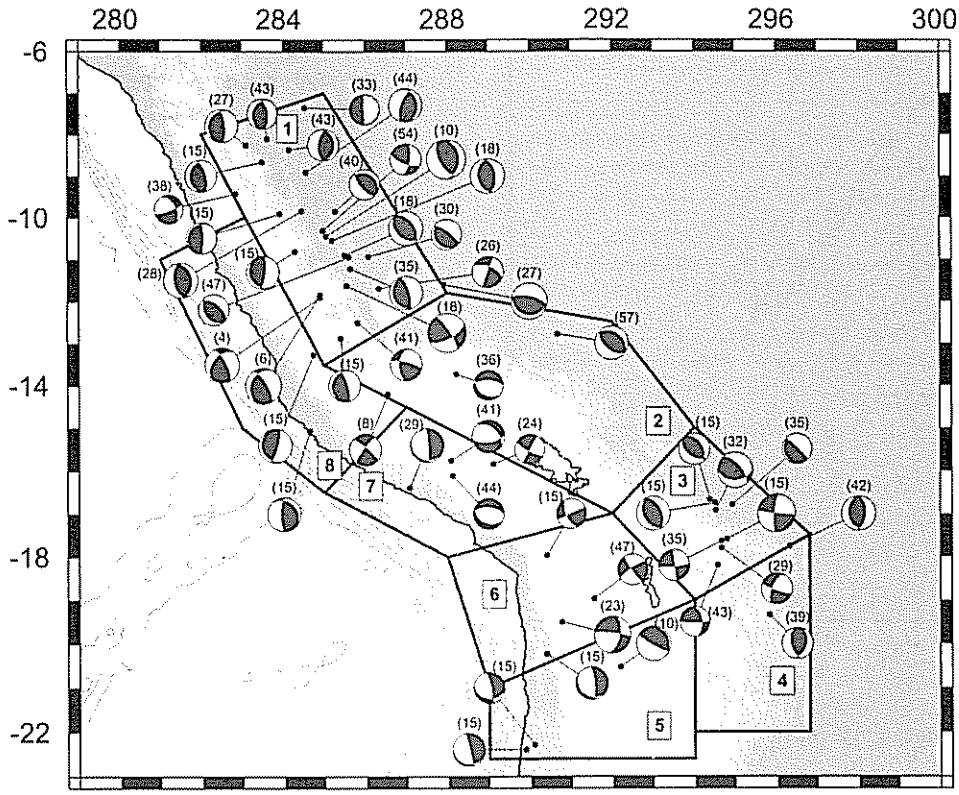

Figure 5. Focal mechanisms for earthquakes in the boundary zone of the South American plate between 0 - 60 km depth and the groups among which they have been divided. Earthquake depth information is in parentheses (km). Data are from *Suarez et al.*, [1983], *Stauder* [1975], and the Harvard CMT moment tensor catalog. Trench contour interval is 1000m. Topography scale is the same as that shown in Figure 1.

similar to those for the thrust events, but have NW-SE oriented T-axes. In group 2, the principal extension axis is more perpendicular to the convergence direction but its magnitude is small due to the low seismicity, and so may not be representative. Because FTB seismicity is concentrated in groups 1 and 3, the seismic strain rates are almost an order of magnitude larger than in groups 2 and 4. The largest magnitude seismic strain rates occur in group 3, consistent with observations of *Lamb* [2000].

Seismic strain rates within the Altiplano/Western Cordillera and coastal regions have principal contraction and extension axes which are less clearly related to the convergence and topography directions. Group 8 shows contraction approximately in the convergence direction, whereas groups 5 and 7 show no clear relation between directions. The principal extension axes (which are horizontal components) are approximately at 90° to their contractional counterparts, except in group 5, where both axes are parallel due to dip-slip faulting on near-vertical planes. In group 6, the principal contraction axis is perpendicular to the coast and the principal extension axis is parallel to the coast. Seismicity in group 6 creates higher strain rates than other Western Cordillera/Altiplano/coastal groups. This is the only group with significant extensional strain oriented NW-SE, due to strike-slip faulting. Thus, the area differs from Cascadia, where geodetic strains show contraction in the convergence direction, whereas earthquake mechanisms show margin-parallel compression [*Wang et al.*, 2000]

5. ASEISMIC SHORTENING?

The most striking difference between the strain rate estimates shown in Figure 3 is that although all three show generally similar directions of shortening, the seismic rates are dramatically lower than those from GPS and geology, which which we view as comparable, given the uncertainties. Hence the seismic shortening rate estimate should also be lower. We estimate the seismic shortening rate, V_{obs}, using

$$V_{obs} = \frac{m_2 \cos(Pl_{m_2})}{2 \mu L z T_{obs}}$$

m_2 is the contractional eigenvalue of the diagonalized seismic moment tensor, associated with the eigenvector whose

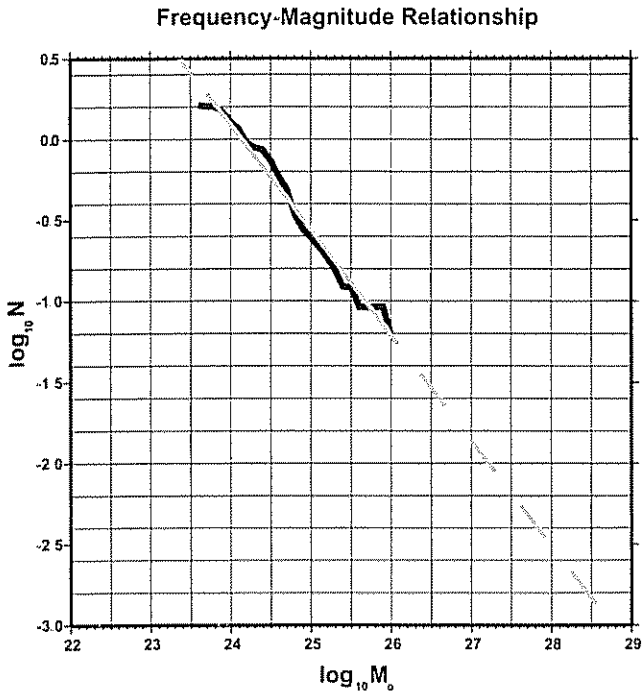

Figure 6. Frequency-magnitude relationship for earthquakes in the study area, plotted as: $\log_{10} N = a - \beta - \log_{10} M_o$, where N is the mean annual occurrence of earthquakes greater than or equal to seismic moment M_o. Earthquake data are plotted with dark line. Linear least-squares fit shown by gray dashed line (a = 15.6 and β = 0.65).

plunge is Pl_{m_2}, L is the length of the seismic zone, and z is the assumed maximum faulting depth (40 km). Shortening rates computed for the FTB are between 0.03-0.42 mm/yr, significantly less than the 10 ± 5 mm/yr from GPS and geology. These rates are even smaller than those (~ 1-1.7 mm/yr) inferred by *Suarez et al* [1983] for a region further north (4° - 16° S), sampling seismicity (1962 - 1978) whose total moment release was approximately four times larger than in our study.

This discrepancy may reflect either a significant component of aseismic shortening, or incompleteness of the short record of earthquakes with known mechanisms. To investigate this issue, we consider the effect of a longer sampling time, assuming that earthquakes in the FTB satisfy the *Gutenberg and Richter* [1954] frequency-magnitude relationship. Written in terms of seismic moments

$$\log_{10} N = a - \beta \log_{10} M_o$$

where M_o is the seismic moment, N is the annual number of earthquakes with moment ≥ M_o, and a and β are the y-intercept and slope of the frequency-magnitude line. For our data (Figure 6) a = 15.6 and β = 0.65.

Although the largest FTB earthquake in our dataset has a moment of 1.25×10^{26} dyne-cm (M_w = 6.7), we use the frequency-magnitude relationship to consider how the shortening estimate would vary if over a longer time interval larger earthquakes with the same average orientation had occurred, such that the moment tensor was simply scaled up in magnitude. Because

$$N = \alpha\ M_o^{-\beta}$$

where α is 10^a, the number of earthquakes within a moment range, n, is

$$n = -\frac{dN}{dM} = \beta\ \alpha\ M_o^{-\beta - 1}$$

(the minus sign is because $N_1 > N_2$ and $M_1 < M_2$). Hence in the time interval T_{scl} by which we expect the largest earthquake to be M_2, the scaled moment release, M_{scl},

$$M_{scl} = T_{scl} \int_{M_1}^{M_2} n\ M_o\ dM_o = T_{scl}\ \beta\ \alpha \int_{M_1}^{M_2} M_o^{-\beta}\ dM_o$$

$$= \frac{T_{scl}\ \beta\ \alpha}{1 - \beta}\left[M_2^{(1-\beta)} - M_1^{(1-\beta)}\right]$$

T_{scl} is determined from the frequency-magnitude relationship (Figure 5) using the reciprocal of the mean annual occurrence of M_2.

The corresponding shortening rate V_{scl} is derived by scaling the inferred shortening rate V_{obs} by the moment release M_{obs} over time T_{obs}, and the predicted moment release M_{scl} over time T_{scl}

$$V_{scl} = V_{obs}\ \frac{M_{scl} / T_{scl}}{M_{obs} / T_{obs}}$$

The ratio V_{scl} / V_{geo}, where V_{geo} (5-15 mm/yr) is the shortening observed geologically and geodetically, indicates the scaled fraction of seismic shortening; no aseismic shortening occurs when this ratio is 1. Figure 7 shows scaled seismic shortening estimates for the FTB. Although the results vary depending on the groups chosen, significant components of aseismic shortening are expected so long as the largest earthquakes do not exceed M_w 8 and in most cases require earthquakes larger than ever observed (the great 1960 Chilean earthquake had M_w 9). Although M_w 8 earthquakes here are not impossible, we consider them unlikely in this tectonic setting. Hence we consider it more likely that most of the shortening occurs aseismically.

6. DISCUSSION

We have considered three different types of data which reflect the crustal shortening in the foreland thrust belt that

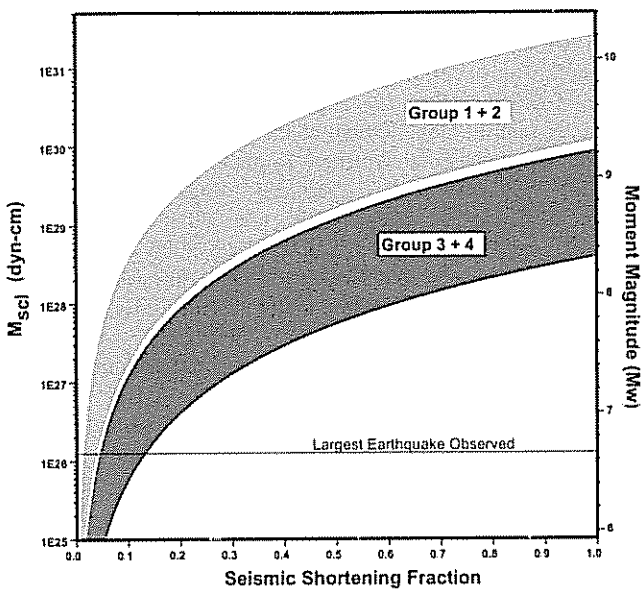

Figure 7. Seismic shortening fraction for northern (groups 1+2) and southern (groups 3+4) FTB assuming that larger earthquakes would occur (estimated from frequency-magnitude relationship of Figure 6). Assumed rate of shortening is 5-15 mm/yr from geologic and geodetic observations. The seismic shortening depends on the assumed magnitude of the largest earthquake and hence, the net moment released.

is currently building the Andes. All three have advantages and limitations.

Estimates from GPS depend on both the velocity field and the model used to interpret it. As the time span of GPS observations increases, the precision of the velocity field will improve, but the shortening estimate will still depend somewhat on the model. At some point it will be possible to confidently resolve along-strike variations. However, although the GPS data can give a very accurate description of the present velocity field, they may span too short a time for useful comparison with the geological data. One possible source of discrepancy can be transient effects of the earthquake cycle. Although the effects of large trench earthquakes are likely to be small, given the distance from the trench, there may be effects from large FTB earthquakes [*Reilinger and Kadinsky-Cade,* 1985]. Even so, it may eventually be possible to determine whether the present shortening rate differs from that averaged over millions of years, as suggested by *Hindle et al.'s* [2002] results that the shortening rate has been accelerating as convergence slows. Given that the GPS data can show the deceleration of plate convergence relative to that averaged over the past 3 Ma, it is not unreasonable that similar analyses can be done within the boundary zone provided the geologic data have sufficient accuracy.

The accuracy of the geologic estimates is hard to assess, given the uncertainties in field observations and interpretation, especially of the timing of deformation. The opportunity to compare these estimates with GPS data may prompt further study and improve estimates. In contrast, the seismic strain rate and hence shortening estimates will be hard to improve significantly except by waiting. These should become better, and probably less variable between different portions of the FTB, over long enough times (hundreds of years or more) that the largest earthquakes occur. Even so, the seismic rate may differ from the geodetic rate if a significant portion of the shortening is aseismic. We suspect that this is the case, given that aseismic deformation has also been inferred for other areas, such as the Zagros, which is part of the Arabia-Eurasia convergent boundary zone [*Jackson and McKenzie,* 1988].

A final point worth noting is that all the data we have discussed address the mountain building process via the associated horizontal motions, which are larger and easier to measure than the actual uplift. The crucial vertical measurements rarely exist except where they can be derived from conventional geodesy using precise leveling [*Jackson and Bilham,* 1994]. Given the effort and difficulties involved, such measurements are rare. Hence there are very few places where we know anything about vertical motion in mountain belts on time scales shorter than tens of millions of years, over which uplift histories can be inferred from various geological techniques [*Gregory-Wodzicki,* 2000; *Burbank and Anderson,* 2000]. Because paleoelevations cannot be measured directly, they are inferred from other factors that vary with elevation, so the different techniques measure different quantities, each with large uncertainties. The lack of direct measurements seriously limits our ability to understand the dynamics of mountain building. Hopefully in years to come vertical motions will be measured using continuous GPS and thus contribute to our understanding of mountain building.

Acknowledgments. We thank R. McCaffrey and P. Chen for useful discussions on the derivation of strain rate formulations. G. Sella provided useful suggestions. Figures were generated using GMT [*Wessel and Smith,* 1991]. This work was supported by NSF grant EAR-0004031 and NASA grant NAG5-10306.

REFERENCES

Allmendinger, R. W., T. E. Jordan, S. M. Kay, and B. L. Isacks, The evolution of the Altiplano-Puna plateau of the Central Andes, *Ann. Rev. Earth Planet. Sci., 25,* 139–174, 1997.

Angermann, D., J. Klotz, and C. Reigber, Space-geodetic estimation of the Nazca-South America Euler vector, *Earth Planet. Sci. Lett., 171,* 329–334, 1999.

Bevis, M., E. Kendrick, R. Smalley, B. Brooks, R. Allmendinger, and B. Isacks, On the strength of interplate coupling and the rate of back arc convergence in the central Andes: An analysis of the interseismic velocity field, *Geochemistry, Geophysics, Geosystems, 2,* 10–129, 2001.

Burbank, D. W., and R. S. Anderson, *Tectonic Geomorphology*, Blackwell Science, 270 pp., 2000

Darwin, C., *The Voyage of the Beagle (1975 reissue)*, J. M. Dent, 432 pp., 1845.

DeMets, C., R. G. Gordon, D. F. Argus, and S. Stein, Effect of recent revisions to the geomagnetic reversal time scale on estimates of current plate motion, *Geophys. Res. Lett., 21,* 2191–2194, 1994.

Dewey, J. F., and J. M. Bird, Mountain belts and the new global tectonics, *J. Geophys. Res., 75,* 2625–2647, 1970.

Dewey, J. F., and S. H. Lamb, Active tectonics of the Andes, *Tectonophysics, 205,* 79–95, 1992.

Feigl, K. L., R. W. King, and T. H. Jordan, Geodetic measurement of tectonic deformation in the Santa Maria fold and thrust belt, California, *J. Geophys. Res., 95,* 2679–2699, 1990.

Gregory-Wodzicki, K. M., Uplift history of the Central and Northern Andes; a review, *Geol. Soc. Am. Bull., 112,* 1091–1105, 2000.

Gubbels, T. L., B. L. Isacks, and E. Farrar, High-level surfaces, plateau uplift, and foreland development, Bolivian central Andes, *Geology, 21,* 695–698, 1993.

Gutenberg, B., and C. F. Richter, *Seismicity of the Earth and Associated Phenomena*, Princeton University Press, 310 pp. 1954.

Hindle, D., and J. Kley, The consistent deformation of the Central Andean plate boundary zone, *Amer. Geophys. Un. Geophys. Monog.*, this volume, 2002.

Hindle, D., J. Kley, E. Klosko, S. Stein, T. Dixon, and E. Norabuena, Consistency of geologic and geodetic displacements during Andean orogenesis, *Geophys. Res. Lett., 29,* 10.1029/2001GL013757, 2002.

Horton, B., Erosional control on the geometry and the kinematics of thrust-belt development in the Central Andes, *Tectonics, 18,* 1292–1304, 1999.

Isacks, B. L., Uplift of the central Andean Plateau and bending of the Bolivian Orocline, *J. Geophys. Res., 93,* 3211–3231, 1988.

Jackson, M., and R. Bilham, Constraints on Himalayan deformation inferred from vertical velocity fields in Nepal and Tibet, *J. Geophys. Res., 99,* 13897–13912, 1994.

Jackson, J., and D. McKenzie, The relationship between plate motions and seismic moment tensors, and the rates of active deformation in the Mediterranean and Middle East, *Geophys. J. R. astron. Soc., 93,* 45–73, 1988.

James, D. E., Andean crustal and upper mantle structure, *J. Geophys. Res., 76,* 3246–3271, 1971.

James, D. E., and I. S. Sacks, Cenozoic formation of the central Andes: a geophysical perspective, *Econ. Geol.*, in press, 1999.

Kley, J., and C. R. Monaldi, Tectonic shortening and crustal thickness in the Central Andes: how good is the correlation? consequences, *Geology, 26,* 723–726, 1998.

Kostrov, V. V., Seismic moment and energy of earthquakes, and seismic flow of rocks, *Izv. Acad. Sci. USSR Phys. Solid Earth, 1,* 23–44, 1974.

Lamb, S., Active deformation in the Bolivian Andes, South America, *J. Geophys. Res., 105,* 25627–25653, 2000.

Lamb, S., and L. Hoke, Origin of the high plateau in the Central Andes, Bolivia, South America, *Tectonics, 16,* 623–649, 1997.

Liu, M., Y. Zhu, S. Stein, Y. Yang, and J. Engeln, Crustal shortening in the Andes: Why do GPS rates differ from geological rates, *Geophys. Res. Lett., 18,* 3005–3008, 2000.

Liu, M., Y. Yang, S. Stein, and E. Klosko, Timescale-Dependent Crustal Shortening and Extension in Central Andes, *Amer. Geophys. Un. Geophys. Monog.*, this volume, 2002.

Mao, A., C. Harrison, and T. Dixon, Noise in GPS time series, *J. Geophys. Res., 104,* 2797–2816, 1999.

Means, W. D., Kinematics, stress, deformation and material behavior, *Jour. of Struct. Geol., 12,* 953–971, 1990.

Molnar, P., and H. Lyon-Caen, Some simple physical aspects of the support, structure, and uplift of mountain belts, *Geol. Soc. Amer. Spec. Paper, 218,* 179–207, 1988.

Norabuena, E., L. Leffler-Griffin, A. Mao, T. Dixon, S. Stein, I. S. Sacks, L. Ocala, and M. Ellis, Space geodetic observations of Nazca-South America convergence along the Central Andes, *Science, 279,* 358–362, 1998.

Norabuena, E., T. Dixon, S. Stein, and C. Harrison, Decelerating Nazca-South America Convergence and Nazca-Pacific Spreading, *Geophys. Res. Lett., 26,* 3405–3408, 1999.

Reilinger, R., and K. Kadinsky-Cade, Earthquake deformation cycle in the Andean back arc, western Argentina, *J. Geophys. Res., 90,* 12,701–12,712, 1985.

Russo, R.M., and P.G. Silver, Cordillera formation, mantle dynamics, and the Wilson cycle, *Geology, 24,* 511–514, 1996.

Schmitz, M., A balanced model of the southern Central Andes, *Tectonics, 13,* 484–492, 1994.

Sella, G. F., T. H. Dixon, and A. Mao, REVEL: A model for recent plate velocities from space geodesy, *J. Geophys. Res., 107,* 10.1029/2000JB000033, 2002.

Sempere, T., G. Herail, J. Oller, and M. G. Bonhomme, Late Oligocene - early Miocene major tectonic crisis and related basins in Bolivia, *Geology, 18,* 946–949, 1990.

Sheffels, B., Lower bound on the amount of crustal shortening in the central Bolivian Andes, *Geology, 18,* 812–815, 1990.

Stauder, W., Subduction of the Nazca plate under Peru as evidenced by focal mechanisms and by seismicity, *J. Geophys. Res., 80,* 1053–1064, 1975.

Suarez, G., P. Molnar, and B. C. Burchfiel, Seismicity, fault plane solutions, depth of faulting, and active tectonics of the Andes of Peru, Ecuador, and southern Colombia, *J. Geophys. Res., 88,* 10403–10428, 1983.

Wang, K., Stress-strain paradox, plate coupling, and forearc seismicity at the Cascadia and Nankai subduction zones, *Tectonophysics, 319,* 321–338, 2000.

Wessel, P., and W. Smith, Free Software Helps Map and Display Data, *Eos Trans. AGU, 72,* 441, 1991.

Yuan, X., S. V. Sobolev, R. Kind, O. Oncken, G. Bock, G. Asch, B. Schurr, F. Graeber, A. Rudloff, W. Hanka, K. Wylegalla, R.

Tibi, C. Haberland, A. Rietbrock, P. Giese, P. Wigger, P. Rower, G. Zandt, S. Beck, T. Wallace, M. Pardo, and D. Comte, Subduction and collision processes in the Central Andes constrained by converted seismic phases, *Nature, 408*, 958–961, 2000.

Zandt, G., S. L. Beck, S. R. Ruppert, C. J. Ammon, D. Rock, E Minaya, T. C. Wallace, and P. G. Silver, Anomalous crust of the Bolivian Altiplano, Central Andes: constraints from broadband regional seismic waveforms, *Geophys Res Lett*, *23*, 1159–1162, 1996.

E.R. Klosko and S. Stein, Department of Geological Sciences, Northwestern University, Evanston, IL 60208.; eryn@earth.nwu.edu, seth@earth.nwu.edu.

D. Hindle, Geoforschungszentrum, Telegrafenberg C223, D-14473, Potsdam, Germany; hindle@gfz-potsdam.de.

J. Kley, Geologisches Institut, Universitaet Karlsruhe, PO Box 6980, D-76128 Karlsruhe, Germany; kley@geo.uni-jena.de.

T. Dixon and E. Norabuena, Rosenstiel School for Marine and Atmospheric Sciences, University of Miami, 4600 Rickenbacker Causeway, Miami, FL 33149.; tdixon@rsmas.miami.edu, enorab@rsmas.miami.edu.

M. Liu, Department of Geological Sciences, University of Missouri, Columbia, MO 65211.; lium@missouri.edu